Proceedings of the ASME 2010 International Mechanical Engineering Congress & Exposition
IMECE2010
November 12-18, 2010, Vancouver, British Columbia, Canada

IMECE2010-40509

BUBBLE DYNAMICS IN A TWO-PHASE BUBBLY MIXTURE

Arvind Jayaprakash
DYNAFLOW INC.
www.dynaflow-inc.com
Jessup, Maryland, USA
arvind@dynaflow-inc.com

Sowmitra Singh
DYNAFLOW INC.
www.dynaflow-inc.com
Jessup, Maryland, USA
sowmitra@dynaflow-inc.com

Georges Chahine
DYNAFLOW INC.
www.dynaflow-inc.com
Jessup, Maryland, USA
glchahine@dynaflow-inc.com

ABSTRACT

The dynamics of a primary relatively large bubble in a water mixture including very fine bubbles is investigated experimentally and the results are provided to several parallel on-going analytical and numerical approaches. The main/primary bubble is produced by an underwater spark discharge from two concentric electrodes placed in the bubbly medium, which is generated using electrolysis. A grid of thin perpendicular wires is used to generate bubble distributions of varying intensities. The size of the main bubble is controlled by the discharge voltage, the capacitors size, and the pressure imposed in the container. The size and concentration of the fine bubbles can be controlled by the electrolysis voltage, the length, diameter, and type of the wires, and also by the pressure imposed in the container. This enables parametric study of the factors controlling the dynamics of the primary bubble and development of relationships between the bubble characteristic quantities such as maximum bubble radius and bubble period and the characteristics of the surrounding two-phase medium: micro bubble sizes and void fraction. The dynamics of the main bubble and the mixture is observed using high speed video photography. The void fraction/density of the bubbly mixture in the fluid domain is measured as a function of time and space using image analysis of the high speed movies. The interaction between the primary bubble and the bubbly medium is analyzed using both field pressure measurements and high-speed videography. Parameters such as the primary bubble energy and the bubble mixture density (void fraction) are varied, and their effects studied. The experimental data is then compared to simple compressible equations employed for spherical bubbles including a modified Gilmore Equation. Suggestions for improvement of the modeling are then presented.

NOMENCLATURE

α	Void fraction
C	Sound speed on bubble surface
c_l	Sound speed of liquid
γ	Surface tension of compressible medium
k	Polytropic gas constant
p	Pressure in fluid domain
P	Pressure at bubble wall
p_g	Bubble gas pressure
p_v	Vapor pressure
R	Bubble radius
$R_{\max}$	Maximum bubble radius
ρ	Density of compressible medium
ρ_l	Liquid density
μ	Viscosity of compressible medium

INTRODUCTION

The spherical dynamics of a bubble in a compressible liquid has been studied extensively since the early work of Gilmore. Numerical codes to study the behavior, including when large non-spherical deformations are involved, have since been developed and have been shown to be accurate. The situation is however different and common knowledge less advanced when the compressibility of the medium surrounding the bubble is provided mainly by the presence of a bubbly mixture. This applies to both when the studied bubble is just one of the bubbles composing the two-phase medium, or in the simpler case where the concerned bubble is much larger than the finer bubbles forming the surrounding medium and is the driving force to the dynamics of this medium. In both cases, modeler resort to simplifying assumptions, with need for validation, and would benefit from a basic fundamental study combining experimental observations and numerical / analytical simulations. This is more so since almost all simulation models use some form of single bubble dynamics as the building block to the two-phase models.

When a proton beam of a Spallation Neutron Source (SNS) impacts the mercury target (see Figure 1) a very high local energy deposition occurs over a very short time period of the order of 0.7 μs. This results in a localized pressure rise of the order of 50 MPa and a subsequent shock or pressure wave propagating away from the energy deposition region. This is followed by a strong expansion wave once the deposited energy recesses. These waves propagate out from the deposition location then reflect from the various SNS target boundaries generating successive compressive and tensile stresses in the mercury and on the container structure. Particularly, the initial expansion wave and the shock wave reflections at the air/steel interface of the SNS stainless steel container result in strong refraction waves, which cavitate the mercury. The resulting cavitation bubbles dynamics and collapses have been shown responsible for measurable erosion of the stainless steel walls [1,2,3]. The rate of the cavitation erosion predicted from preliminary controlled tests is such that it will effectively limits the lifespan of the target vessel to a few months at normal operation. This has prompted the Oak Ridge National Laboratory (ORNL) which operates the SNS to devise means to improve this lifespan.

In order to mitigate the cavitation damage, several options have been investigated including the injection of microbubbles containing non-condensable gas in the bulk of the liquid mercury and/or creating a protective air layer near the threatened stainless steel wall. The presence of microbubbles and/or an air layer would allow the mercury to expand more freely when the proton energy is deposited, thus absorbing the energy of the expansion wave and reducing the amplitude of the high pressures reaching the steel/air interface (and thus the reflected expansion waves responsible for cavitation) by exploiting the acoustic properties of bubbles to attenuate the shock/pressure waves as they propagate in the two-phase medium. In addition, an air layer that would persist during the dynamics would prevent cavitation bubbles from collapsing at the stainless steel walls and thus from damaging it. On the other hand, as is often the case with injected bubbles in a cavitating flow field, the injected bubbles themselves could result in enhanced cavitation activity instead of mitigation, and the air layer could become disrupted and result in cavity collapse if the design is not good. It is presently not clear, which bubble sizes or size distributions are required to achieve the desired mitigation.

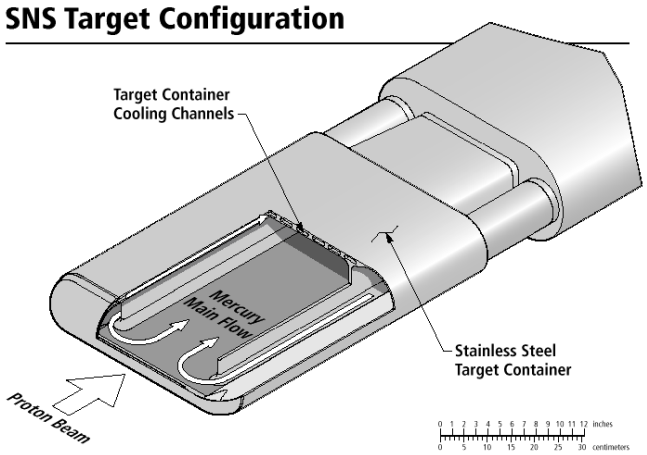

Figure 1. Schematic of the mercury target in the ORNL SNS system [1].

Bubble Dynamics

When gas bubbles encounter large negative pressure gradients, they grow explosively and then on encountering high pressure, they collapse violently generating shock waves. In the absence of gravity effects or nearby objects, a bubble remains spherical, and its volume oscillations can be predicted analytically. Rayleigh [4] analyzed the collapse of an empty spherical cavity and found the time the cavity requires to collapse was:

$$\tau_{collapse} = 0.915 R_{\max} \sqrt{\frac{\rho}{P_{amb}}}, \qquad (1)$$

where R_{max} is the initial maximum radius of the cavity, and ρ and P_{amb} are the density and pressure of the ambient fluid. The effect of vapor pressure, non-condensable gas, surface tension, and a time-varying ambient pressure were then included, to produce the Rayleigh-Plesset equation [4-5] the equation of the wall motion for a collapsing and rebounding spherical bubble. For given conditions, the full dynamics of the bubble oscillations can be predicted from this equation. Using the unsteady Bernoulli equation, one can then predict the pressure in the liquid around the bubble.

To better understand the dynamics of interaction of strong pressure wave in a two-phase bubbly medium, a canonical set-up is selected to study the dynamics of a primary relatively large bubble in a water mixture including very fine bubbles. For ease of visualization, a hemispherical bubble is generated at rigid transparent wall. Using the principle of images, this set-up models a spherical bubble in an infinite bubbly medium. More details of the set-up are discussed in the following section. The schematic of the geometry along with the parameters involved is shown in Figure 2.

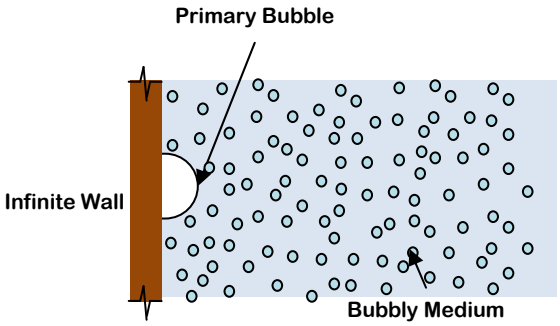

Figure 2. Definition sketch of the parameters of the problem of a primary bubble in bubbly medium.

This study of dynamics of a primary bubble in a two-phase mixture is conducted as a combined experimental and numerical task. This paper addresses the experimental part of the study. A numerical part is presented as a sister paper in this conference [6].

The objectives of the present studies are as follows:

a. Experimentally investigate the dynamics of a primary bubble in two-phase mixture by performing simulations encompassing a wide range of cases.
b. Characterize the bubble evolution for different void fractions and bubble energy.
c. Measure bubbly media effect on pressure propagation.
d. Validate some of the preliminary numerical simulations with the obtained experimental data.

EXPERIMENTAL SET-UP

An effective method to study the dynamics of single primary bubble in bubbly medium is the use of electric spark generated bubbles in a container where the ambient pressure can be controlled. Spark generators have been used for studying bubbles in a liquid for quite a long time [9-14]. DYNAFLOW, INC. has several test chambers that can be used to simulate full-scale bubble dynamics, and is equipped with flow diagnostics tools including high speed photography and pressure measurement capabilities.

The use of high speed cameras to photograph spark-generated bubbles produces high quality observations of bubble dynamics including clear visualizations of reentrant jet formation inside the bubble. Such observations can be extremely useful in developing and validating numerical models.

Spark Bubbles Generation

Spark generated bubbles at DYNAFLOW are generated by the underwater discharge of a high-voltage charge between two coaxial electrodes contained within a transparent cell. The underwater spark discharge is a process by which electrical energy is converted into small volume plasma which has temperatures as high as 20,000^{o}K, and pressures as high as 10,000 atmospheres [10]. As the trigger pulse breaks down the hold-off gap between electrodes, current flows between the electrodes with energy being absorbed in the plasma at a rate depending upon the power input and the inertia of the water. Eventually, due to a decrease in the voltage and an increase in the ionization, temperature, and pressure of the plasma, the spark is extinguished. The energy is initially stored in the plasma in the form of dissociation, excitation, ionization, and kinetic energy of the constituent particles. While the heated and pressurized plasma will tend to expand, the inertia of the outside water will tend to confine it. Mechanical work, light radiation, thermal radiation, and thermal conduction dissipate the energy from the plasma at a rate slower than energy input from the spark [10].

Because of the high pressure, the liquid near the plasma interface is initially compressed. This high pressure leads to the formation of a shock wave that radiates outward. The energy in the shock wave comprises 20 to 50 percent of the energy imparted by the spark into the water [10]. After emission of the shock wave, the pressure in the gas sphere quickly falls, but remains well above that of the surrounding liquid. The pressure difference, however, is small enough that compressible effects can be neglected. From this point on, incompressible hydrodynamic effects dominate. The pressurized gas expands into a large bubble which subsequently collapses and re-expands. The phenomena preceding the incompressible hydrodynamic phase occur quickly and are accompanied by light generation that prevents accurate determination of the initial bubble radius using conventional high-speed photography.

The bubble period is modified by controlling the pressure above the free surface in the test cell. Decreasing the value of P_{cell} increases R_{max} and thus effectively increases the bubble period. Increasing the bubble radii and slowing down the bubble collapse helps in better visualization and which in turn help producing high fidelity data. Larger bubble period enables

better data sampling rate in data acquisition, i.e., more data points can be used to represent the quantity recorded.

Another way to increase the bubble size, R_{max} is to increase the energy at spark discharge. The energy of the bubble is controlled by adjusting the voltage supplied to the capacitor of the spark generator and/or by modifying the capacitor. In cases where the bubble is significantly distant from boundaries, it retains an almost spherical shape through the time of its maximum volume and a radius could be easily measured.

In cases where the bubble is distorted by the presence of boundaries, an equivalent radius based on the measured volume can be used. Here, it was obtained for each case by assuming the bubble to be axisymmetric, and calculating its volume as the volume of a solid of revolution of the observed outline around its vertical axis.

The ambient pressure was measured using the atmospheric pressure in the vacuum cell and the hydrostatic head computed using the depth of the electrodes, and the vapor pressure was deduced from the measured ambient water temperature.

To generate the bubbly medium a wire mesh electrolyser was used. Electric current is applied across the electrolyser and results in dissociation of water into oxygen and hydrogen. Increasing the current increases the number of microbubbles produced. The microbubble size distribution roughly depends upon the diameter and the density distribution of the electrolyser mesh.

The transparent walls allowed recording of the bubble dynamics by a high-speed digital camera (Redlake Imaging model PCI8000S). The acoustic signals of the bubbles were measured with a quartz transducer having a 1μs rise time and resonance frequency $\simeq$430 kHz (PCB Piezotronics model 102A03).

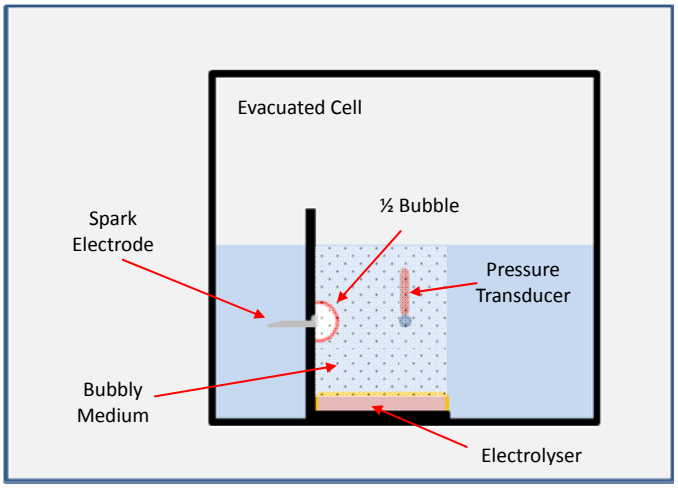

Figure 3. Schematic of a DYNAFLOW's spark cell set-up.

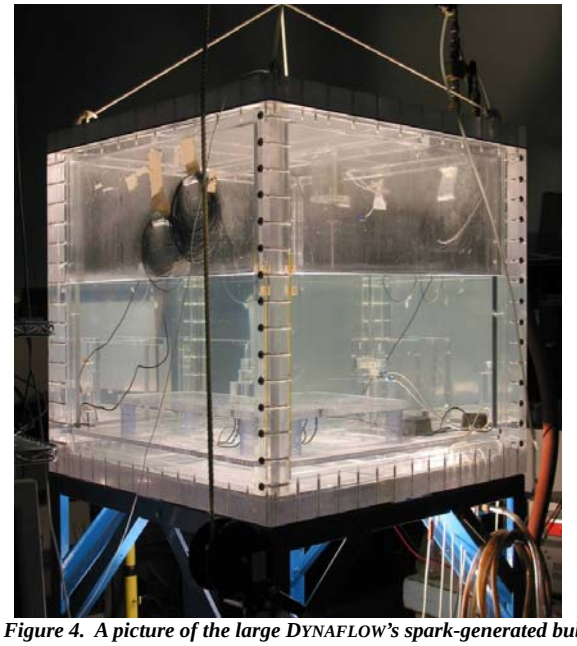

Figure 4. A picture of the large DYNAFLOW's spark-generated bubbles test facility. The Plexiglas tank dimensions are 1m x 1m x 1m and the wall thickness is 2.5 cm.

NUMERICAL METHOD

The present numerical study is based on solving an analytical second order ordinary differential equation for wall-motion of the primary bubble in consideration. This differential equation, derived by Gilmore [7], applies to a spherical bubble in a compressible medium. In the current study, the compressibility effects of the surrounding bubbly medium, assumed to be continuous, are taken into account by using an equation of state (describing the pressure-density relation that exists in a bubbly medium) to modify and compute relevant parameters appearing in the differential equation.

Spherical Bubble dynamics

The equation governing the interface dynamics of a spherical bubble in a compressible liquid can be written as follows [7].

$$\left(1-\frac{\dot{R}}{C}\right)R\ddot{R}+\frac{3}{2}\left(1-\frac{\dot{R}}{3C}\right)\dot{R}^2=H\left(1+\frac{\dot{R}}{C}\right)+\frac{R\dot{H}}{C}\left(1-\frac{\dot{R}}{C}\right). \quad (2)$$

In the above equation, R is the radius of the spherical bubble, C is the sound speed at the bubble surface and H is the enthalpy difference in the compressible medium between the bubble surface and the medium at infinity. The above equation was derived with the assumption that the density of the medium can be expressed as a function of the pressure only [7].

Additionally, the flow in the medium is assumed to be spherically symmetric and hence irrotational.

Thermodynamically, the quantity H can be given by the following relation [7],

$$H = \int_{P_\infty}^{P} \frac{dp}{\rho}, \tag{3}$$

where ρ is the local density of the compressible medium, P_∞ is the pressure at infinity, p is the pressure in the medium at location r and P is the pressure at the bubble wall. The pressure in the liquid at the bubble wall can be related to the pressure inside the bubble and the surface tension γ.

$$P = p_v + p_g - \frac{2\gamma}{R}. \tag{4}$$

p_v is the vapor pressure of the medium/liquid and p_g is the pressure of the gas in the bubble. Vaporization is assumed to occur at a very short time scale so that, p_v is assumed to remain constant inside the bubble. The gas inside the bubble is assumed to obey the polytropic compression law [7]:

$$p_g = p_{g0}\left(\frac{R_0}{R}\right)^{3k}. \tag{5}$$

k in the above equation is the polytropic gas constant, p_{g0} is the initial gas pressure inside the bubble – corresponding to a bubble radius of R_0.

If an equation describing the pressure-density relationship for a medium is known, the above equations can be solved to obtain the variation of bubble radius with time.

a. Enthalpy expansion in pure water

For pure water, the pressure-density relation for isentropic compression can be given by the following Tait [4] expression:

$$\frac{p+B}{P_\infty + B} = \left(\frac{\rho}{\rho_\infty}\right)^n, \tag{6}$$

where ρ_∞ in the above expression is a reference density corresponding to a pressure P_∞. B and n are known constants ($B \approx 3000\ atm$, $n \approx 7$ for water). Using(6), the sound speed at a point in the fluid domain can be expressed as follows:

$$c^2 = \frac{dp}{d\rho} = \frac{n(p+B)}{\rho}. \tag{7}$$

Using (6) and (7), the sound speed at the bubble surface can be expressed by the following relation:

$$C = c_\infty \left(\frac{P+B}{P_\infty + B}\right)^{\frac{n-1}{2n}}. \tag{8}$$

In the above equation, c_∞ is the reference sound speed corresponding to the reference pressure P_∞. Similarly, using (3) and(6), one obtains the following expression for H:

$$H = \frac{n(P_\infty + B)}{(n-1)\rho_\infty}\left[\left(\frac{P+B}{P_\infty + B}\right)^{\frac{n-1}{n}} - 1\right] \tag{9}$$

As mentioned earlier, once H and C on the bubble surface are known, the system of equations describing the wall-motion dynamics of a spherical bubble can be solved.

b. Enthalpy expansion in the bubbly medium

The sound speed in a compressible bubbly medium can be expressed as follows [8]:

$$c^2 = \frac{p}{\rho_l}\frac{\left[1 + \frac{\alpha}{1-\alpha}\right]^2}{\left[\frac{1}{k}\frac{\alpha}{1-\alpha} + \frac{p}{\rho_l {c_l}^2}\right]} \tag{10}$$

In deriving the above relation, it is assumed that:

- the density of the gas is negligible relative to the density of the liquid, ρ_l,
- the disperse gas phase obeys the polytropic compression law (k being the polytropic gas constant),
- surface tension is absent at the interface of the two components (p varies smoothly in the medium) and
- the void fraction, α, is small.

c_l in relation (10) is the sound speed in the pure liquid. Also, the density of the compressible medium can be written as follows:

$$\rho = \rho_m \sim \rho_l(1-\alpha). \tag{11}$$

Relation (10) can be integrated to obtain the equation of state (relating pressure and density/void-fraction) for the bubbly medium [8]:

$$\frac{\alpha}{1-\alpha} = \left[\frac{\alpha_0}{1-\alpha_0} + \frac{k}{k+1}\frac{p_0}{\rho_l {c_l}^2}\right]\left(\frac{p_0}{p}\right)^{\frac{1}{k}} - \frac{k}{k+1}\frac{p}{\rho_l {c_l}^2}. \tag{12}$$

In the above equation, α_0 is a reference void-fraction corresponding to a reference pressure p_0. In our computations, we have assumed $p_0 = P_\infty$. Equation (12) can be re-written as follows:

$$\frac{\alpha}{1-\alpha} = f(p) = \left(A + D\right)\left(\frac{p_0}{p}\right)^{\frac{1}{k}} - D\frac{p}{p_0} \tag{13}$$

where, $A = \frac{\alpha_0}{1-\alpha_0}$ and $D = \frac{k}{k+1}\frac{p_0}{\rho_l {c_l}^2}$.

This equation can be also expressed as:

$$\frac{1}{1-\alpha} = 1 + f(p). \tag{14}$$

Using the definition of H and writing the density of the medium in terms of the density of the liquid and the void-fraction (relation(11)), we have:

$$H = \int_{P_\infty}^{P} \frac{dp}{\rho} = \int_{P_\infty}^{P} \frac{1}{\rho_l(1-\alpha)} dp. \tag{15}$$

Using relation(14), we obtain:

$$H = \int_{P_\infty}^{P} \frac{1+f(p)}{\rho_l} dp. \tag{16}$$

Carrying out the integration, we have:

$$H = \frac{P - P_\infty}{\rho_l} + (A+D)\frac{k}{\rho_l(k-1)} p_0^{\frac{1}{k}} \left(P^{\frac{k-1}{k}} - P_\infty^{\frac{k-1}{k}} \right) - \frac{D}{2p_0\rho_l}\left(P^2 - P_\infty^{\,2} \right). \tag{17}$$

Also, note that for a given bubble wall pressure, P, C on the bubble surface can be obtained using equations (10) and (12).

RESULTS AND DISCUSSION

Two sets of scaled spark tests, each repeated 3 times, are presented here with conditions. One set is in absence of electrolysis injected bubbles and the second is in the bubbly medium as tabulated in Table 1.

Shown in Figure 5 and Figure 7 are time snapshots from high-speed movies of primary spark bubble growing and collapsing in the "pure" liquid and in the bubbly medium.

Using image analysis techniques, the bubble outlines were extracted from the recorded high-speed movies of the spark tests. Then, the volume of the bubble was computed as the volume of a body formed by revolving the observed outline around its horizontal axis. Finally, the bubble equivalent radii were computed by using the bubble volume.

Presented in Figure 8 and Figure 9 are the primary bubble equivalent radii vs. time for the two sets of experiments conducted in pure liquid (i.e., no bubble injection, but clearly some other nuclei were present in the water at all times) and bubbly medium. Repeatability variations of the primary bubble equivalent radii are attributed to small change in the ambient pressure in the evacuated cell and mostly to the known non perfect repeatability of spark discharge [10]. This influence can be mitigated by normalizing the data [13,14].

Case	Scaled Spark Test Parameters				
	Electrode Depth (cm)	Bottom Depth (cm)	Ambient Pressure (mBar)	Spark Strength (kV)	Bubbly Medium
1	12	24	174	6	No
2	12	24	174	6	No
3	12	24	174	6	No
4	12	24	172	6	Yes
5	12	24	171	6	Yes
6	12	24	171	6	Yes

Table 1. List of experiments carried out in the spark cell.

Normalizing the equivalent radii with the maximum radius of the bubble, R_{max} and the time with Rayleigh-time, $t_{rayleigh}$ based on R_{max} and the experimental ambient pressure [defined in (1)], collapses the curves over each other. Shown in Figure 10 and Figure 12 are the normalized primary bubble equivalent radii evolution. In pure water, the non-dimensional curves collapse very well, while in the bubbly medium the collapse is less perfect, most probably due to the non-exact conservation of the bubbly medium void fraction between the cases.

Overall, Figure 11 and Figure 13 show the comparisons of primary bubble radii evolution in pure liquid and in bubbly medium. We can observe from Figure 11 that clearly the primary bubble in the case of the experiments conducted in bubbly medium did not grow as much as the primary bubble radii of the ones that were conducted in pure liquid. This clearly can be attributed as an effect of the presence of the bubble distribution on the evolution of primary bubble.

Another effect of the bubbly medium observed from the normalized curves shown in Figure 13, is that the rate at which the bubble collapses, when in bubbly media is decreased i.e., the primary normalized bubble period is increased and the slope of the normalized radius vs. time is also decreased. This phenomenon, along with the reduced R_{max}, is what primarily affects the violence of the primary bubble collapse and in turn reduces the magnitude of the spike in the field pressure observed during primary bubble collapse.

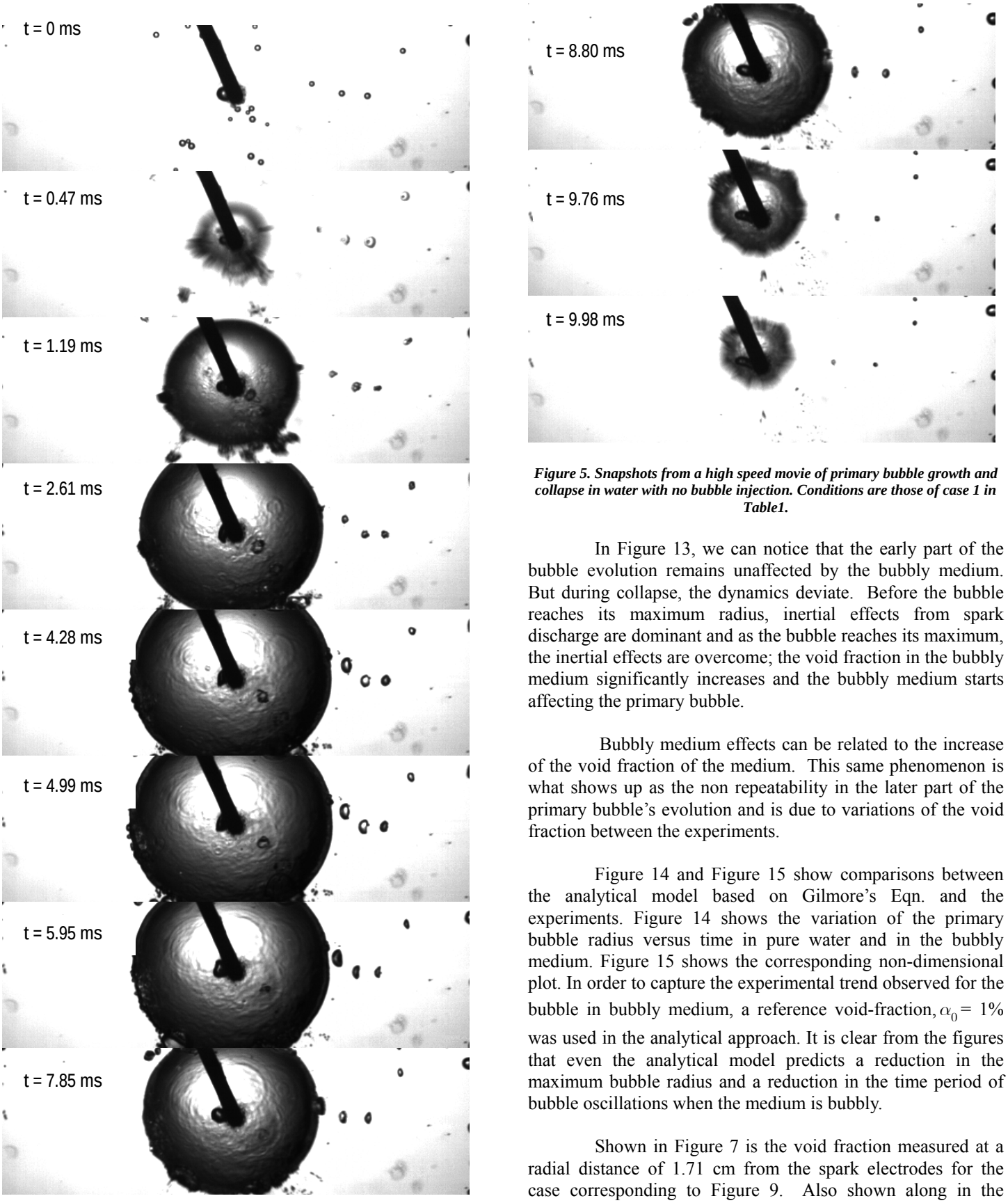

Figure 5. Snapshots from a high speed movie of primary bubble growth and collapse in water with no bubble injection. Conditions are those of case 1 in Table1.

In Figure 13, we can notice that the early part of the bubble evolution remains unaffected by the bubbly medium. But during collapse, the dynamics deviate. Before the bubble reaches its maximum radius, inertial effects from spark discharge are dominant and as the bubble reaches its maximum, the inertial effects are overcome; the void fraction in the bubbly medium significantly increases and the bubbly medium starts affecting the primary bubble.

Bubbly medium effects can be related to the increase of the void fraction of the medium. This same phenomenon is what shows up as the non repeatability in the later part of the primary bubble's evolution and is due to variations of the void fraction between the experiments.

Figure 14 and Figure 15 show comparisons between the analytical model based on Gilmore's Eqn. and the experiments. Figure 14 shows the variation of the primary bubble radius versus time in pure water and in the bubbly medium. Figure 15 shows the corresponding non-dimensional plot. In order to capture the experimental trend observed for the bubble in bubbly medium, a reference void-fraction, $\alpha_0 = 1\%$ was used in the analytical approach. It is clear from the figures that even the analytical model predicts a reduction in the maximum bubble radius and a reduction in the time period of bubble oscillations when the medium is bubbly.

Shown in Figure 7 is the void fraction measured at a radial distance of 1.71 cm from the spark electrodes for the case corresponding to Figure 9. Also shown along in the

Figure 7, is the void fraction computed at the same location using the analytical method. It can be noticed that the experimental void fraction measurements show fluctuations and the analytical computation appear smoothed. This is due to the fact that the experiment captures the dynamics of individual microbubbles, which grow and collapse based on their initial radii, in response to its local encounter pressure. While the analytical model does not take into account the discrete microbubbles dynamics, rather, it expresses only the void fraction of a continuum bubbly medium.

Overall, comparisons between experiments and the analytical model are quite good until the end of the primary bubble collapse. In that phase of the dynamics, a close look at the experiments shows that gravity plays an important role and the bubble deviates from a spherical shape and migrates upwards. This is obviously not the case in the analytical model.

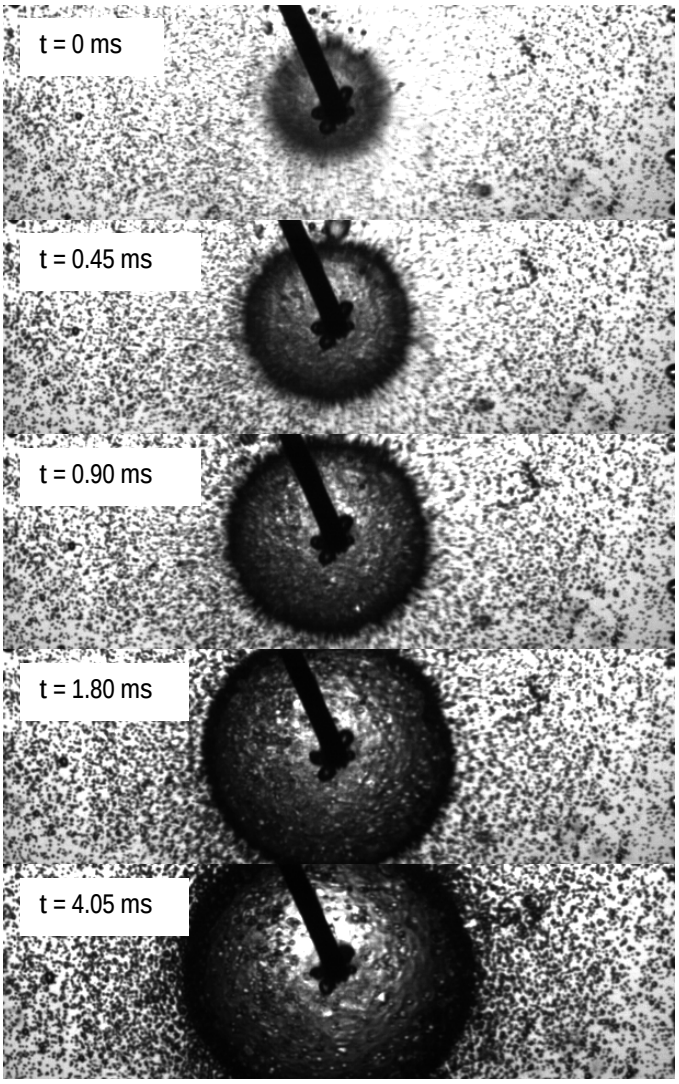

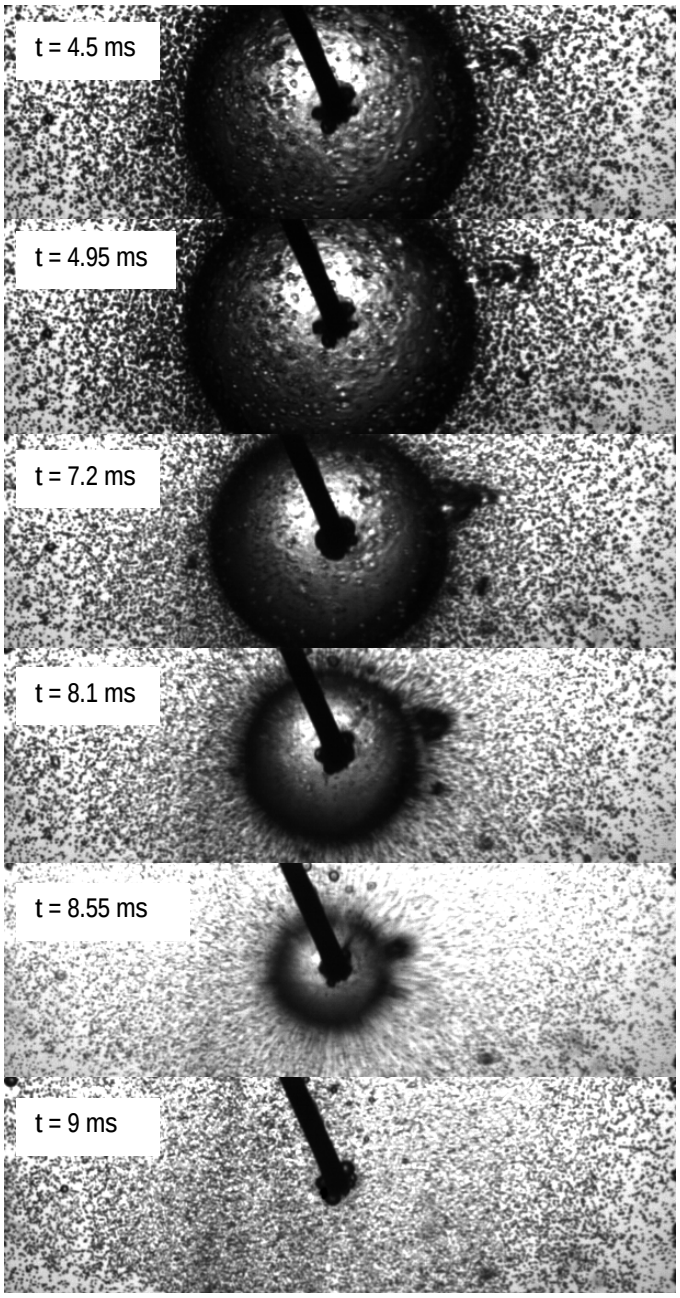

Figure 6. Snapshots from a high speed movie of primary bubble growth and collapse in water with bubble injection. Conditions are those of case 4 in Table1.

The pressure transducer was located at a radial distance of 11 cm from the spark electrode tip on the wall. Shown in Figure 16 and Figure 17 are comparisons of the field pressure observed in pure liquid and in bubbly medium. Noticeably, the presence of bubbly medium has mitigated the pressure wave originating from the bubble collapse.

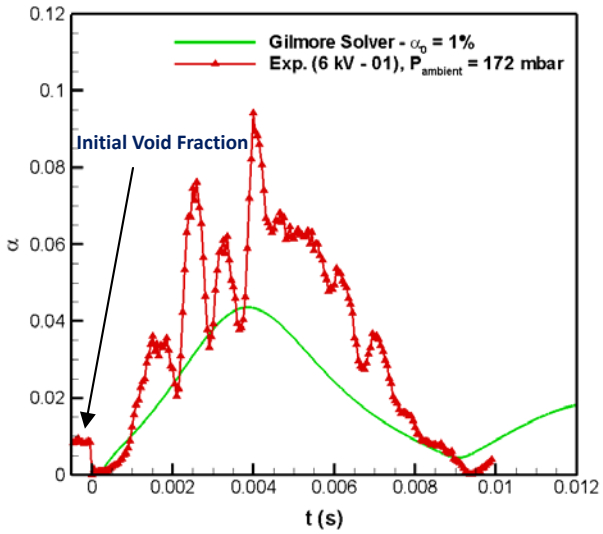

Figure 7. Comparison of void fraction computed from experiments and analytical model at 1.71cm from spark electrode.

Finally, more experiments and pressure measurements under various conditions are being made to further corroborate the findings so far. Also, to gain confidence in the image analysis method of void fraction estimation, experiments are currently being conducted using our instrumentation called the ABS Acoustic Bubble Spectrometer®. The ABS is an acoustics based device that measures the void fraction and bubble size distribution based on sound speed attenuation due to bubbly media [15].

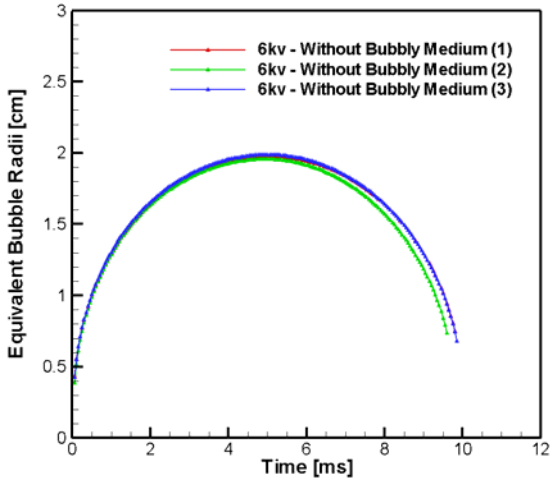

Figure 8. Evolution of the primary bubble radii vs. time for the set of experiments conducted in pure water. Conditions 1,2,3 in Table 1.

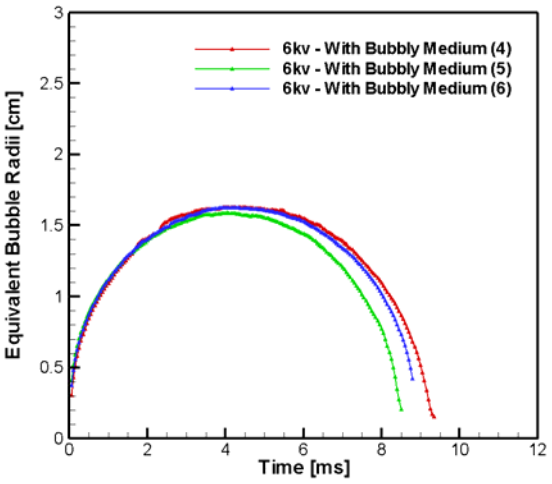

Figure 9. Evolution of the primary bubble radii vs. time for the set of experiments conducted in a bubbly medium. Conditions 4,5,6 in Table 1.

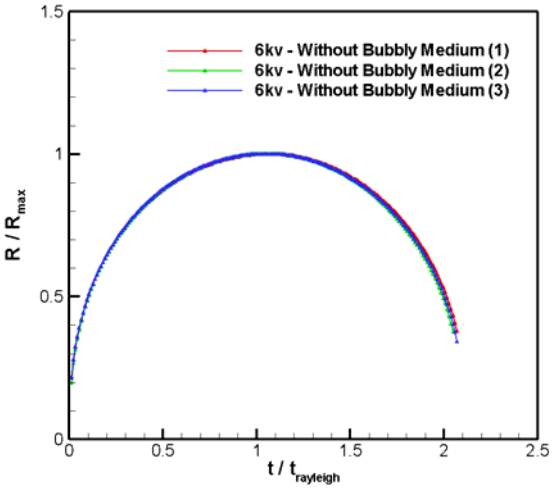

Figure 10. Evolution of normalized primary bubble radii vs. time for the experiments conducted in pure liquid.

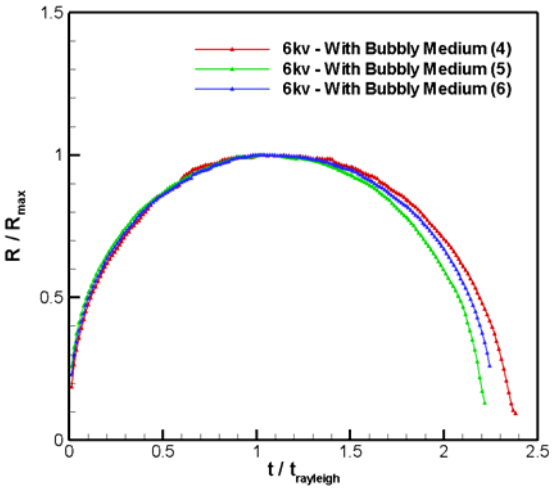

Figure 11. Evolution of normalized primary bubble radii vs. time for the experiments conducted in bubbly medium.

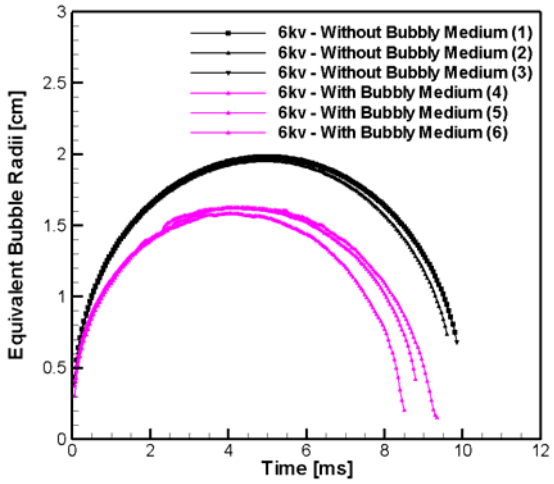

Figure 12. Comparisons of evolution of primary bubble radii vs. time for the experiments conducted in pure liquid and bubbly medium.

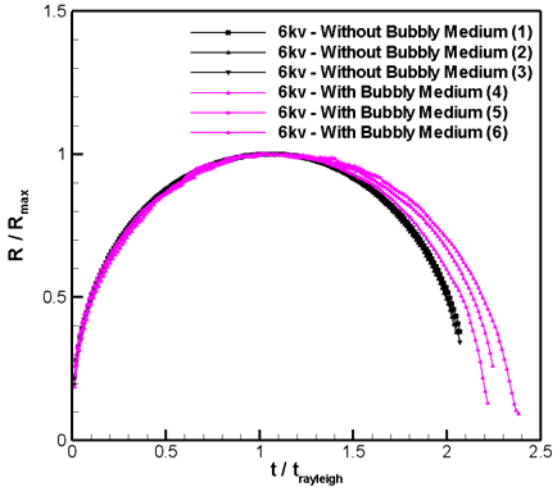

Figure 13. Comparisons of evolution of normalized primary bubble radii vs. time for the experiments conducted in pure liquid and bubbly medium.

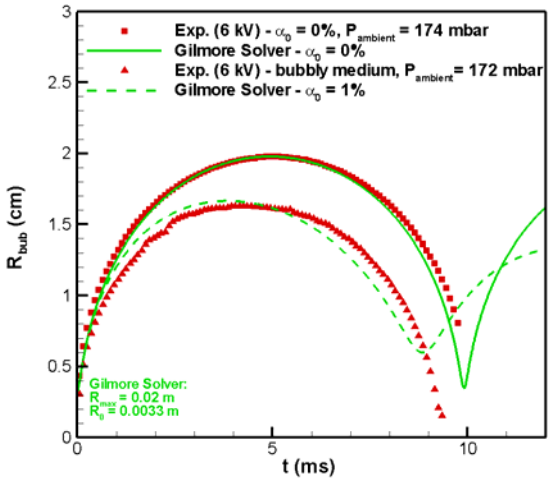

Figure 14. Evolution of primary bubble radii vs. time – Experiments versus Analytical Model. Experimental data are average of the 3 experiments and void fractions used are 0% and 1%.

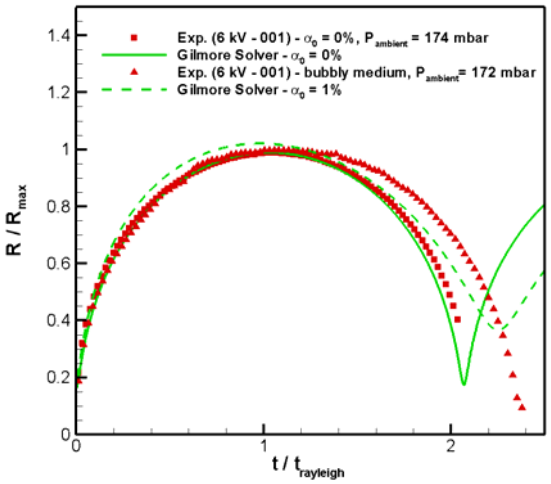

Figure 15. Evolution of the normalized primary bubble radii vs. time (normalized) – Experiments versus Analytical Model.

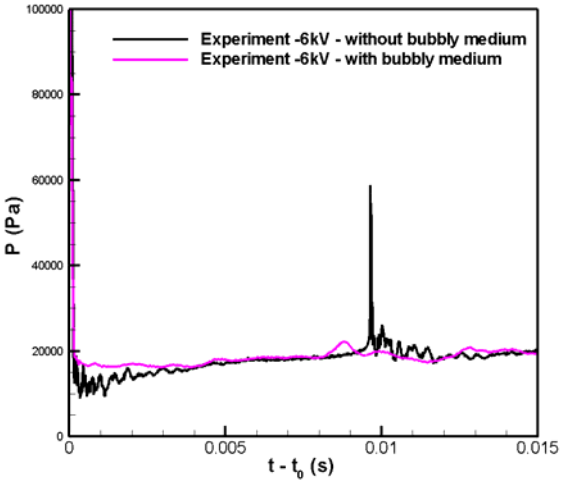

Figure 16. Monitored pressure from transducer located at 11 cm from bubble center versus time – Experiments.

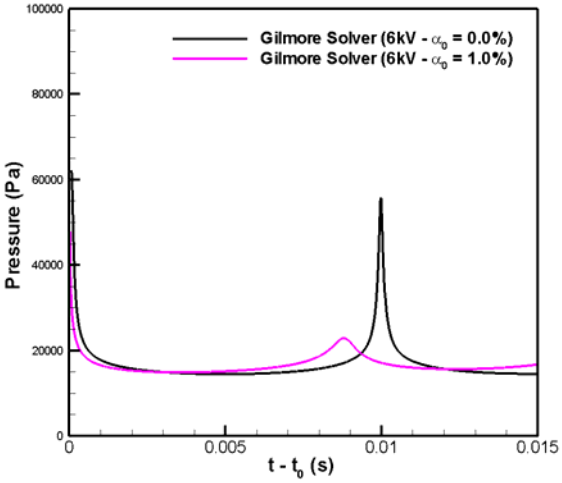

Figure 17. Monitored pressure at r = 11cm versus time – Analytical Model. Bubble initial conditions are R_0 = 0.0033 m and P_{g0} = 1512942 Pa.

CONCLUSIONS

In order to better understand the effect of a bubbly medium on the dynamics of a primary bubble, experiments were conducted with a spark generated hemispherical bubble near a rigid transparent wall, in both pure liquid and in bubbly medium.

The evolutions of the primary bubble radius in pure and a bubbly medium were compared. It was shown that the presence of the bubbly medium dampens the growth of the primary bubble and slows down the rate of bubble collapse.

The experimental data was used to compare against an analytical model developed based on Gilmore's Equation. The model was also able to capture the same trend as seen in the experiments.

Finally, with preliminary data both from the experiments and the analytical model, the mitigation effects of a bubbly medium were qualitatively confirmed.

To further strengthen the claims, more experiments are being conducted with spark bubbles of different sizes, ambient pressures and void fractions. Also, the image analysis method of void fraction computation is being refined and will be validated with the use of the ABS - Acoustic Bubble Spectrometer®.

ACKNOWLEDGEMENTS

Support for this work was provided by the Department of Energy (DOE) under contract DE-FG02-07ER84839. Support from the Office of Naval Research (ONR) under contract N00014-09-C-0676, Dr. Ki-Han Kim – Monitor, is also acknowledged.

The authors would also like to acknowledge the efforts of Philippe Amorim (Intern, DYNAFLOW, INC.), Emmanuel Coleman (Technician, DYNAFLOW, INC) and Richa Mann (Research Scientist, DYNAFLOW, INC) in helping us with the spark bubble experiments and data analysis.

REFERENCES

1. Mitigation of Cavitation Damage in Liquid Metal Spallation Targets," Workshop, Oak Ridge National Laboratory, TN, Jan 24-26, 2008.
2. Riemer, B. W. "Benchmarking Dynamic Strain Predictions of Pulsed Mercury Spallation Target Vessels," *Journal of Nuclear Materials*, 343, pp. 81-91, 2005.
3. Manzi. N., Chitnis. P., Holt. R., Roy. R., Cleveland. R., Riemer, B., and Wendel. M., "Detecting cavitation in mercury exposed to a high-energy pulsed proton beam", *The Journal of Acoustical Society of America*, Vol. 127, No. 4, April 2010.
4. Rayleigh, L. "On the pressure developed in a liquid during the collapse of a spherical cavity", Phil. Mag. 34, 94-98, 1917.
5. Plesset, M. "The dynamics of cavitation bubbles", *ASME Journal of Applied Mechanics*, 16, 228-231, 1949.
6. Raju, R., Singh, S., Hsiao, C.-T., and Chahine, G. L. "Study of Strong Pressure Wave Propagation in a Two-Phase Bubbly Mixture", IMECE2010-40525, *ASME 2010 International Mechanical Engineering Congress & Exposition*, Vancouver, British Columbia, November 10-12, 2010.
7. Gilmore, F. R. "The Growth and Collapse of a Spherical Bubble in a Viscous Compressible Liquid", California Institute of Technology, Div. Rep. 26-4, Pasadena, CA, 1952.
8. Brennen, C.E. "Cavitation and Bubble Dynamics", Oxford University Press, 1995.
9. Ellis, A. T. "Parameters Affecting Cavitation and Some New Methods for Their Study," California Institute of Technology, Rep E-115.1, 1965.
10. Kling, C.L. "A High Speed Photographic Study of Cavitation Bubble Collapse," *Ph.D. thesis*, University of Michigan, Ann Arbor, 1970.
11. Blake, J.R. and Gibson, D.C. "Cavitation Bubbles Near Boundaries," *Annual Review of Fluid Mechanics*, vol. 19, pp. 99-123.
12. Chahine, G. L. "Etude Locale du Phénomène de Cavitation Analyse des Facteurs Régissant la Dynamique des Interfaces," *Docteur ès Sciences Thesis*, University Paris VI, 1979.
13. Chahine, G. L., Duraiswami, R., and Lambrecht, C.J. "A method for validation of Underwater Explosion Bubble Codes: The Use of Benchmark Observations for Spark Generated Bubbles", *Dynaflow Inc. Technical Report 6.002-18*, June 1994.
14. Chahine, G. L., Frederick, G.S., Lambrecht, C., Mair, H. and Harris, G. S. "Spark-generated bubbles as laboratory-scale models of underwater explosions and their use for validation of simulation tools," *SAVIAC Proceedings of the 66th Shock and Vibrations Symposium*, Volume I, Biloxi, MS, 1995.
15. Duraiswami, R., Prabhukumar, S. and Chahine, G.L. "Bubble Counting Using and Inverse Acoustic Scattering Method", *Journal of the Acoustical Society of America*, Vol 104 (5), pp. 2699-2717, 19